Applications of geophysical inversions in mineral exploration

Douglas W. Oldenburg, Yaoguo Li, and Colin G. Farquharson, University of British Columbia
Peter Kowalczyk, Placer Dome, Incorporated, Vancouver, British Columbia
Theo Aravanis, CRA Exploration, Toronto, Ontario
Alan King and Ping Zhang, INCO Exploration and Technical Services, Copper Cliff, Ontario
Anthony Watts, Falconbridge Limited (Exploration), Falconbridge, Ontario

Increases in computing power and advances in mathematical optimization theory have combined to produce a new generation of algorithms that can invert geophysical data to recover 1-D, 2-D, or 3-D images of the earth's physical properties. These images may indicate mineralization directly or delineate the associated structures. In both cases they are valuable aids to mineral exploration, and they provide information that previously had to be distilled from data maps alone. In this short article, we illustrate both the practicability of inverting geophysical data and the important, even decisive, information that it provides. Applications are in time-domain electromagnetics, DC resistivity and induced polarization, gravity, and magnetics.

Before embarking upon examples, we present the main aspects of our inversion methodology. In a typical inverse problem we are provided with observations, some estimate of their uncertainties, and a relationship that enables us to compute predicted data for any model (m). The model represents the spatial distribution of a physical property such as electrical conductivity, magnetic susceptibility, chargeability, or density. Our goal is to find the m which gave rise to the observations. The principal difficulty is nonuniqueness: the observations provide only a finite number of constraints on m and if one model acceptably fits the observation, there are assuredly many more. A fundamental question is therefore, "Of all the models that fit the observations, which one should the inversion algorithm construct?" The constructed solution should have a "character" that emulates the local geology and should be interpretable. This can be achieved by designing an "appropriate" model objective function, and finding the m which minimizes this function while adequately reproducing the observations. We require our generic model objective function to be simple in its number of free parameters, and yet, since one geologic environment can differ dramatically from another, flexible enough to generate models of widely differing character. Our objective function is therefore composed of a term that can force the constructed model to be close to a reference model, and terms which penalize roughness of structure in each spatial direction. Additional weighting functions can also be included for specialized purposes. (See "Suggestions for further reading" to find the explicit form of the objective function, along with a fuller account of our inversion methodology.) With the control given by the flexibility of the objective function, the user can incorporate a priori information about the model into the inversion, generate a preferred model, test the necessity of particular structures in an inverted image, and explore nonuniqueness.

To solve the inverse problem numerically, we divide the earth into cuboidal cells and assume that the physical property of interest is constant within each cell. The cells are sufficiently small that the discretization does not affect the final solution. (This makes our formalism different from parametric approaches to solving the inverse problem.) The "model" then becomes a vector, and the inverse problem is solved by minimizing the model objective function subject to the constraints that the observed data be reproduced. Unfortunately, the observations are not perfectly accurate, and this raises the next important question, "What are the uncertainties in the observations?" or the corollary, "How well should the data be reproduced?" Different measures of misfit are possible. We mostly use a sum-of-squares measure. We assume that the observations are contaminated with Gaussian noise, and that an estimate of the standard deviation of noise in each datum is available. Then the misfit has an expected value equal to the number of data, and our solution of the inverse problem is obtained by mini-

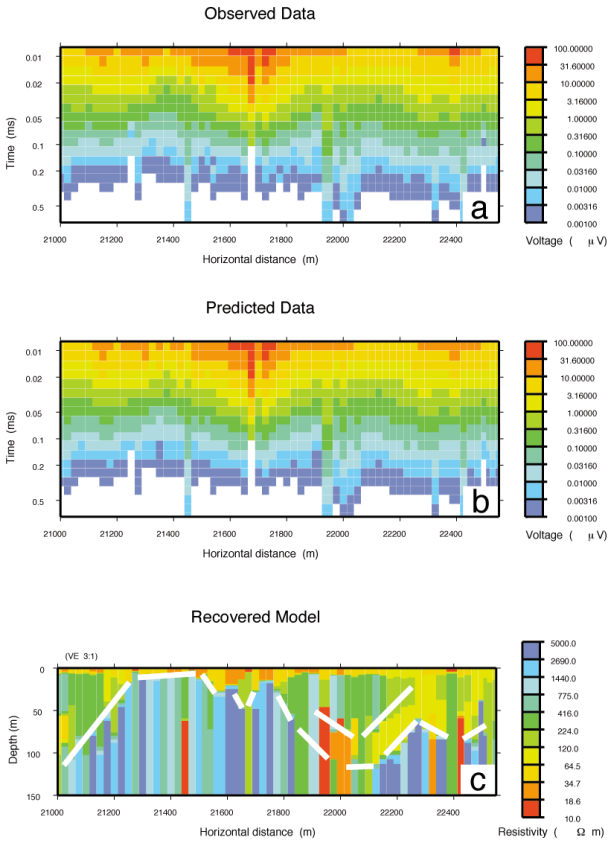

Figure 1. (a) Observed TEM data along one survey line at the Las Cristinas gold project. (b) Predicted data for the models recovered from the inversion. (c) Resistivity section made by concatenating the 1-D models from each sounding along the line. The broken white line indicates the base of the weathered saprolite layer, and, between 21 900 and 22 300 m, the top of the relatively conductive layer associated with the acidic oxide-sulfide mixture which is a feature of mineralization systems in this region.

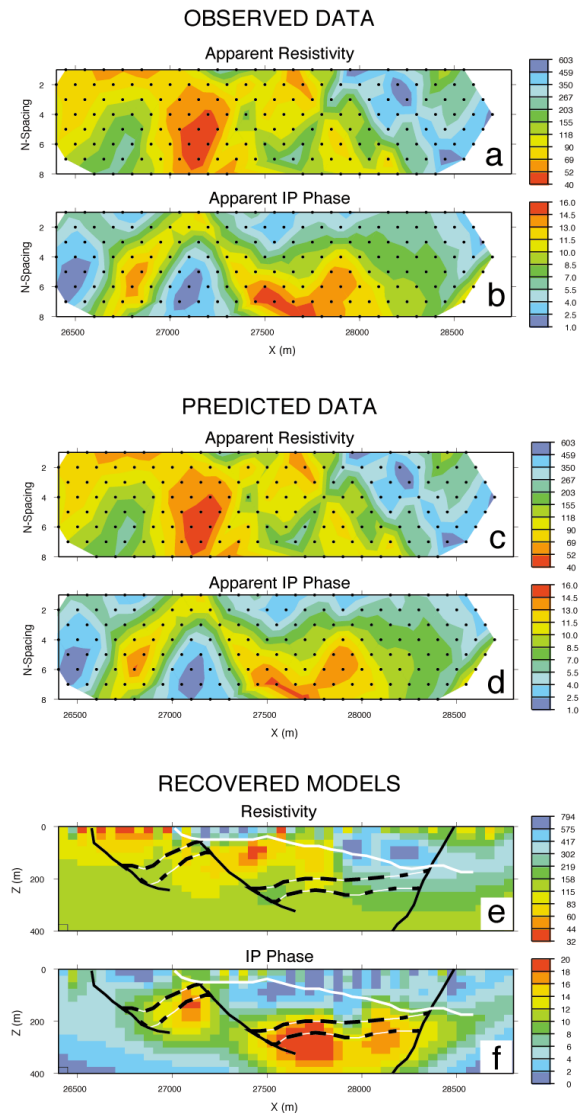

Figure 2. DC and IP inversion of line 47 000E at Century deposit. (a) Apparent resistivity pseudosection. (b) Apparent IP phase pseudosection. Color scales indicate the resistivity in Ω-m and phase in mrad. (e) Inverted resistivity section. (f) Inverted phase section. Overlaid are the boundary of the overburden (white line), three faults (black lines), and the boundaries of the ore body (dashed lines). (c) and (d) show the predicted data from the models at the bottom.

mizing the model objective function subject to adequately fitting the observations. Because of the uncertainty in knowing the true standard deviations, the recovered model may be deemed too rough or too smooth. A subsequent inversion with a modified value of the target misfit can then be performed to construct a more acceptable model.

If the relationship between the model parameters and the data is linear, the solution to the inverse problem is obtained by solving a single matrix system of equations. In the more usual case in which the relationship is nonlinear, an iterative procedure is required. At each iteration a system of equations is constructed and solved to give a perturbation that updates the model. The solution to the inverse problem is obtained once the iterative procedure has converged to the model that both minimizes the model objective function and fits the observations to the target value.

Applications to field data. The inversion algorithms used in the examples presented here were developed under the auspices of the consortium for Joint and Cooperative Inversion of Geophysical and Geological Data (JACI). The algorithms have been made available to the sponsors, and the following "mini" case histories have been provided by them. In some instances the data have also been reinverted at the UBC Geophysical Inversion Facility using algorithms undergoing further development. The examples presented in this paper include time domain electromagnetic (TEM) data from Las Cristinas, DC resistivity and induced polarization (IP) data from the Century deposit, magnetic data from Raglan, and gravity data from Voisey's Bay. They illustrate our inversion methodology in 1-D, 2-D, and 3-D.

1-D inversion of TEM data from Las Cristinas. The features typical of a mineralized system in this Venezuelan gold project are a deepening of the weathered saprolitic layer, a low resistivity zone associated with an acidic oxide-sulfide mixture at the base of this weathered layer, and a high-resistivity zone at the top of the weathered layer due to clays altered by the hydrothermal activity. A total of 5000 TEM soundings were acquired. A Geonics Protem 47 transmitter attached to an 8-turn, 5×5 m loop was used in conjunction with a high-frequency receiver coil system. Data were recorded 20 m from the center of the transmitter loop. The interval between soundings was 25 m. The ramp turnoff time was 10 µs, and 20 time channels of data were

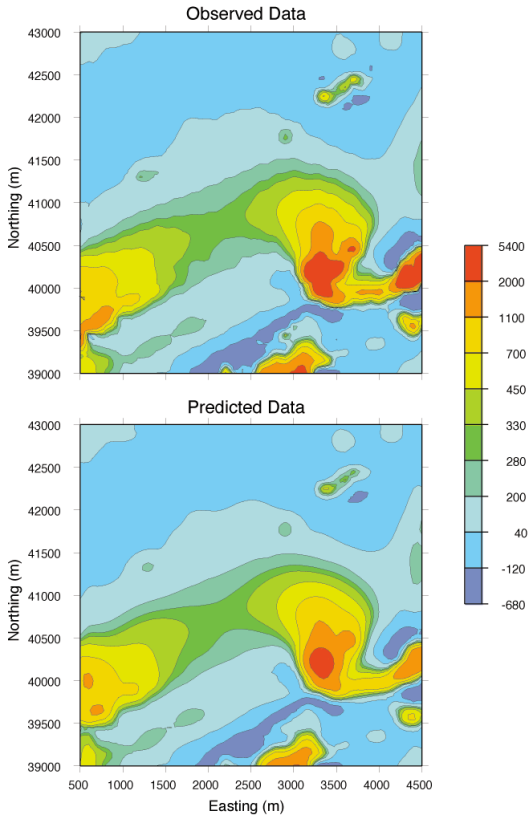

Figure 3. The top panel shows the total field aeromagnetic data. The inducing field has I = 83° and D =-32°. Data are contoured in nT, but the peak value near the magnetic high toward the southeast corner exceeds 5000 nT. The lower panel is the predicted data from the 3-D magnetic inversion. The observed and predicted data show visible differences around the outcrops, but they agree very well away from the outcrops.

recorded. In the first phase of the interpretation, the data were transmitted by satellite to Placer Dome in Vancouver, inverted, and the interpreted conductivity models returned, by satellite, to the field. The inversion of each sounding used the 1-D algorithm of Farquharson and Oldenburg (1993). The model was discretized into 30 horizontal layers of successively increasing thickness, and the logarithm of conductivity was used as the model parameter. The model objective function penalized structure in the vertical direction. Since this particular inverse problem is nonlinear, an iterative solution was necessary. Estimated measurement uncertainties varied from approximately 1% for the earliest time channel to approximately 20% for the latest time channel. The 1-D models for all the soundings along a survey line were concatenated into a 2-D section.

The observed data for a single line are shown in Figure 1a. The resistivity section obtained from the inversion algorithm, which has been slightly modified to generate a more "blocky" structure, is shown in Figure 1c. Data predicted from the resistivity models are shown in Figure 1b. The large contrast between the conductive saprolite and the resistive bedrock shows up as a reasonably well-defined boundary in the resistivity section. The variable depth of this boundary as it appears on the section has subsequently

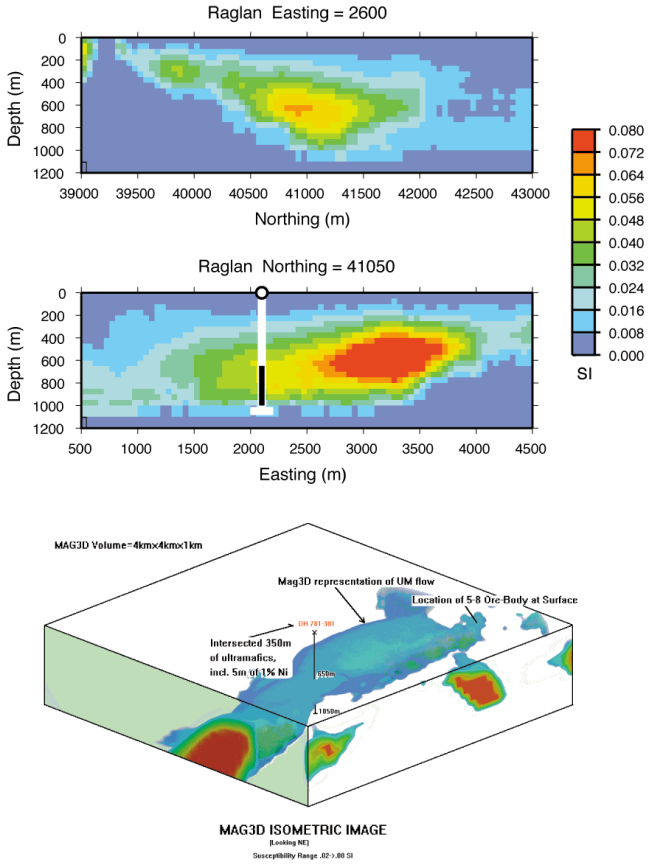

Figure 4. 3-D susceptibility model recovered from magnetic inversion at Raglan deposit. The upper panel shows two sectional cuts through the model. The susceptibility is plotted in SI units as indicated by the color bar. The lower panel is a volume-rendered image of the inverted susceptibility model, and the displayed surface provides a representation of the ultramafic flow. Indicated in the east-west section and in the volume-rendered representation is the intersecting drill hole that was spotted based upon the inversion result.

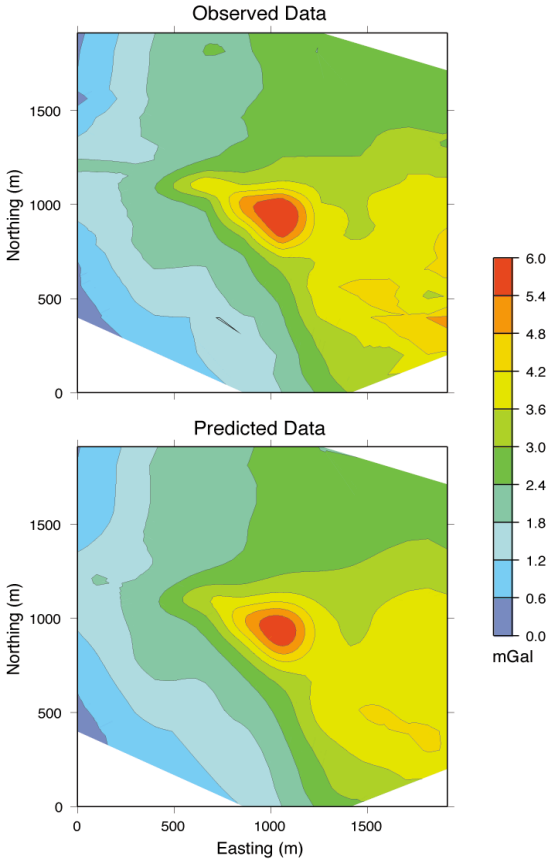

Figure 5. The top panel shows the observed Bouguer gravity anomaly. Data are contoured in mgal. The lower panel is the predicted data from the 3-D gravity inversion.

been verified by drilling. Of particular importance is the trough in the bedrock topography from 21 900 to 22 300 m. The low-resistivity region at the base of the weathered saprolite and the more resistive zone above are the typical features of a mineralized system in this region.

2-D inversion of DC resistivity and IP data at Century deposit. The Century deposit, approximately 250 km north-northwest of Mt. Isa in northwest Queensland, Australia, is hosted by relatively flat-lying middle Proterozoic siltstone and shale units. Mineralization occurs preferentially within black shale units as fine-grained sphalerite and galena with minor pyrite. Complex resistivity dipole-dipole data were collected over the deposit and inverted by CRA Exploration. Apparent resistivity and IP pseudosections for line 47 000E are shown in Figure 2a and 2b. The 177 data are inverted using the algorithm described in Oldenburg and Li (1994). The earth is assumed to be 2-D and is divided into 2000 rectangular cells each having a constant resistivity and chargeability. First the DC resistivity data are inverted. Data are assigned a 3% error, and the objective function is designed to generate a model that is equally smooth in the horizontal and vertical directions and tends to return to the reference model of 10 Ωm at depth where the data no longer constrain the model. The inversion is nonlinear, and iterations are required. The variable for the inversion is logρ. The recovered model is shown in Figure 2e along with a superposed geologic section. The inversion nicely delineates the resistive overburden of limestones on the right. The resistivity at depth is not correlated with mineralization. This conclusion is

supported by subsequent borehole logging which measured the resistivities of the ore zone in the range of 100-300 Ωm, and the host siltstone and shales to have resistivities of 60-80 Ωm. The measured resistivity of the limestones was in excess of 1000 Ωm.

The resistivity model in Figure 2e is used to calculate the sensitivity matrix for inversion of the IP data. The model discretization for IP inversion is the same as for DC resistivity. The reference model is zero, and data are ascribed an error of 0.5 mrad. The chargeability model, with geologic overlay, is shown in Figure 2f. The IP inversion has delineated the horizontal extent and depth to the orebody. It also indicates a major fault between x=27 000 m and x=27 500 m that dislocates the ore sequence. The chargeable body on the inverted section is somewhat thicker than drill hole results. This occurs for two reasons. Our objective function constructs smooth models, and hence discrete boundaries will appear as gradational images. Also, downhole IP and petrophysical data indicate that while Century ore is strongly polarizable, the adjacent units, particularly the footwall sediments, are weakly chargeable. This adds to the response and thickens the region of polarization. Overall, the IP image provides important information about both mineralization and structure.

3-D inversion of magnetic data at Raglan. Total field magnetic data taken over the Raglan deposit in northern Quebec are shown in Figure 3a. Two regions of high magnetic field are observed. These coexist with ultramafic outcrops, and the geologic question was whether the outcrops were associated with a single flow unit. For the 3-D inversion the earth was modeled with a $40 \times 40 \times 10$ grid of cells (16 000 cells); the horizontal dimensions of the cells were 100×100 m. The data are assumed to have noise of 2% plus 5 nT. The objective function is designed to make the constructed model smooth in all three spatial directions and also close to a zero reference model. Positivity is included in the inversion. We neglect remanent magnetism and self-demagnetization effects but require that the susceptibility be positive. The procedure outlined in Li and Oldenburg (1996) is used. A crucial aspect of their inversion is the incorporation of a depth weighting of the form

$$w(z) = \frac{1}{(z + z_0)^3}$$

into all components in the objective function, where z_o is a constant dependent upon the observation height and the size of model cells. This counteracts the natural $1/r^3$ decay of the magnetic kernels and allows the inversion to distribute the susceptibility in depth. The recovered model, provided by Falconbridge, was obtained after 25 iterations. Almost all of the misfit occurs at the outcrops. The 100 × 100 m cells are simply too large to handle the extreme variability of the near-surface magnetic susceptibility. However, the data outside these outcrops are adequately reproduced, as shown in Figure 3b.

An important aspect of 3-D inversion is the ability to display a 3-D model. A 3-D cube of susceptibilities can be displayed in cross-sectional cuts or as a 3-D-isometric image after volume rendering. Cross-sectional cuts have the advantage that the value of the physical property in each cell is displayed. These are the numbers which reproduce the field data and from which quantitative questions can be answered. North and south cross-sections are provided in Figure 4. The disadvantage of the cross-sections is that it is sometimes difficult to get a sense of 3-D structure. This is where 3-D volume-rendered images have an

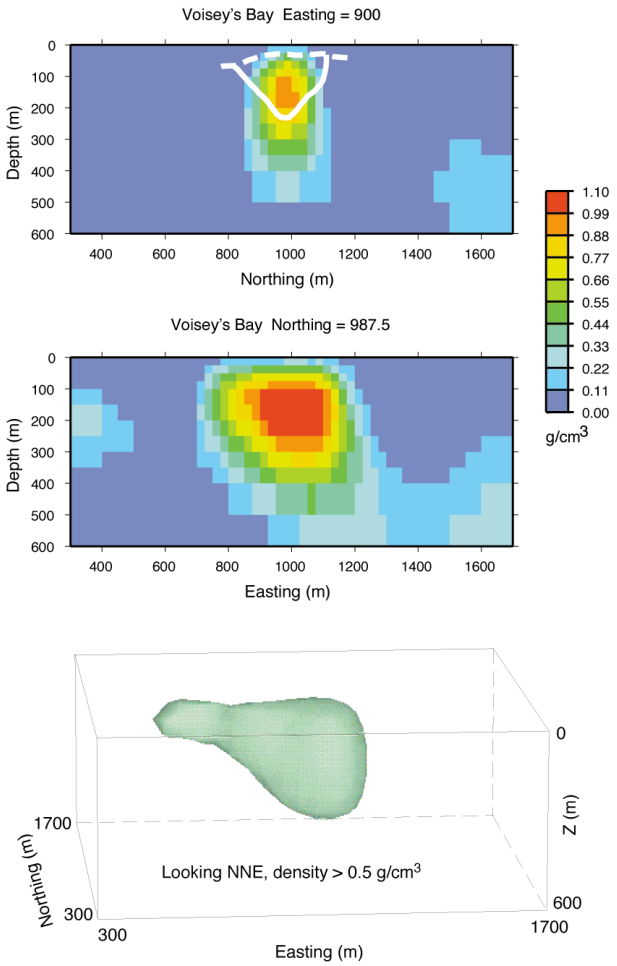

Figure 6. 3-D model of density contrast recovered through the 3-D inversion of gravity data at Voisey's Bay deposit. The top panel shows two sectional cuts through the center of the inverted 3-D density model. The boundary of the overburden (dashed line) and the outline of the ovoid body (solid line) are also overlaid in the north-south section. The scale indicates density in g/cm³. The lower panel shows a volume-rendered image of the 3-D density anomaly. The cutoff value is 0.5 g/cm³.

advantage, but care must be taken since a different threshold for volume rendering will generate a different image. In Figure 4, we also present the 3-D isometric image generated by Falconbridge. The threshold level is about .04 so susceptibilities less than that are transparent. It was this image that persuaded the project geologist to spot the deep 1100-m hole and provided confidence that the apparently isolated outcrops on the "5-8 Ultramafic Flow and the Katinniq flow" to the west were in fact connected at depth. The targeted magnetic source was intersected at 650 m. As a bonus, a 10-m mineralized section (sub-ore grade, approximately 1% Ni) was intersected within the 350-m thick intersection of magnetic ultramafics.

3-D inversion of gravity data at Voisey's Bay. Gravity data were collected over INCO's "Ovoid" ore body at the Voisey's Bay deposit in Labrador, Newfoundland. 3-D inversion of gravity data is similar to the 3-D inversion of magnetic data with the primary difference being in the exponent for the depth weighting function. The field from an elementary mass falls off as $1/r^2$ rather than $1/r^3$ as it does in magnetics. Correspondingly the depth weighting

$$w(z) = \frac{1}{(z + z_0)^2}$$

is used in the algorithm of Li and Oldenburg (1998). The earth was modeled as 38 000 cells. The cell dimension varies from 25 m in the central region to 200 m toward the edge. The objective function is designed to produce a model that is smooth in three spatial directions, and the reference model is set to zero. Positivity is included in the inversion. A total of 1900 Bouguer anomaly data are inverted to recover the density model, and the assumed error is 3% plus 0.01 mGal. The inversion converged to the desired misfit. The observed and predicted data are shown in Figure 5. In Figure 6 we show the final model in the central region of the inversion, which encloses the Ovoid ore body. The cross-section at 900 m north shows a region of high density at the location of the ore body, whose thickness increases from the west to the east. The recovered density has a maximum of 1.0 g/cm^3 in this section, but it reaches 1.4 g/cm^3 in other sections. This is consistent with the knowledge that the massive sulfide body has a maximum density of 4.5 g/cm^3, and the density of the host is 2.8 g/cm^3. From the inversion model, INCO estimated a depth to the top of the ore body to be 30 m. This is slightly larger than the general overburden thickness of 10-20 m but quite realistic since the thickness of near-surface cells was 25 m. The lower part of Figure 6b is a volume-rendered image of the 3-D density model with a cutoff value of 0.5 g/cm^3. This image provides a good representation of the geometry of the ore body and justifies its name "Ovoid."

Conclusion. In this paper we have implemented a single methodology to invert geophysical data to recover 1-D, 2-D, or 3-D distributions of an appropriate physical property. The two greatest problems in implementing the geophysical inversions are:

- specifying the model objective function to be minimized, and
- specifying the misfit functional and deciding how well to fit the data.

When careful attention is paid to these aspects, it is possible for the inversion algorithm to provide meaningful and valuable information about the earth. The field examples validate this comment, and it is hoped they will be a motivating force to ensure that all geophysical data are ultimately inverted.

Suggestions for further reading. "Inversion of time-domain electromagnetic data for a horizontally layered earth" by Farquharson and Oldenburg (*Geophysical Journal International*, 1993). "3-D inversion of magnetic data" (GEOPHYSICS, 1996), "3-D inversion of gravity data" (GEOPHYSICS, 1998) by Li and Oldenburg. "Inversion of induced polarization data" by Oldenburg and Li (GEOPHYSICS, 1994), and Web site http://www.eos.ubc.ca/ubcgif. TLE

Acknowledgments: This work was supported by an NSERC IOR grant and the industry consortium Joint and Cooperative Inversion of Geophysical and Geological Data. Participating companies are Placer Dome, BHP Minerals, Noranda Exploration, Cominco Exploration, Falconbridge, INCO Exploration & Technical Services, Hudson Bay Exploration and Development, Kennecott Exploration Company, Newmont Gold Company, Western Mining Corporation, and CRA Exploration Pty.

Corresponding author: Doug Oldenburg, email doug@eos.ubc.ca